Chemeca 2016
25 – 28 September 2016, Adelaide, Australia

An X-ray Tomography Study of Gas Retention in Nuclear Legacy Waste

M. Johnson*[1], J. Peakall[2], M. Fairweather[1], S. Biggs[3], D. Harbottle[1], T.N. Hunter[1]

[1] School of Chemical and Process Engineering, University of Leeds, Leeds, LS2 9JT, UK
[2] School of Earth and Environment, University of Leeds, Leeds, LS2 9JT, UK
[3] School of Chemical Engineering, University of Queensland, Brisbane, Qld 4072, Australia

*Corresponding author. Email: pm12mcj@leeds.ac.uk

Abstract: The retention and release of flammable gases from corroded Magnox sludge waste at Sellafield, UK and secondary reprocessing waste at Hanford, USA has significant economic and safety implications for decommissioning various nuclear legacy buildings. Magnesium hydroxide is the primary precipitation product from the corrosion of first generation nuclear fuel in the UK, with hydrogen gas produced as a reaction by-product. Depending on the bed microstructure, wettability and shear yield stress behaviour, some consolidated sediments of these corrosion products are able to trap a substantial volume of gas, sufficient in some instances to become buoyant with respect to a water supernatant, resulting in an undesirable upward transfer of radioactive material from the consolidated bed. These phenomena are investigated using the decomposition of hydrogen peroxide to produce oxygen bubbles within magnesium hydroxide soft sediments at laboratory scale. X-ray tomography analysis showed that high strength sediments of 1112 Pa shear yield stress supported much larger bubbles up to 20 mm equivalent spherical diameter than beds in the 7-234 Pa range, which demonstrated almost identical bubble size distributions across the range. The largest retained bubbles became progressively more distorted with increased sediment strength until the lateral cracks consistent with tensile fracture became apparent in the 1112 Pa bed. These cracks significantly limited the capacity for bed swell as gas diffusion along the cracks to the container walls provided a continuous escape route. The capacity for gas retention was also substantially reduced when gas generation was not homogeneous through the bed as localised gas generation promoted the formation of low density pathways, rich with micro-bubbles, which enable gas transport through the bed.

Keywords: nuclear waste, Magnox, gas retention, tomography

1 Introduction

Decommissioning first generation Magnox-era nuclear legacy buildings is a priority activity for the Sellafield nuclear site, accounting for a quarter of its £2billion annual budget [1]. Long term underwater storage of Magnox clad fuel since the 1960s has allowed the magnesium/aluminium cladding alloy to corrode, with precipitation products consolidating into a legacy of corroded Magnox sludge waste [2, 3]. Corrosion of these cladding materials and radiolysis reactions also generate flammable gases in various legacy nuclear waste environments:

$$Mg + 2H_2O \rightarrow Mg(OH)_2 + H_2 \quad (1)$$

The expansion and contraction of consolidated legacy wastes in response to changes in ambient pressure has confirmed significant accumulation of gas within waste tanks at Hanford, USA and storage silos at Sellafield, UK [4, 5]. Further observations at Hanford have periodically revealed significant upward transfers of decay heat from the consolidated waste layer coinciding with spikes in hydrogen concentration in the tank ullage, leading to safety concerns associated with large episodic releases of flammable gas [6]. These episodic releases are understood to occur in particularly high voidage beds where the bulk density falls below that of a convective supernatant, resulting in Rayleigh-Taylor style instabilities [7].

Gas retention also has significant economic implications for the interim storage and ultimate disposal strategy for these wastes [1]. Waste swell increases the required capacity of containers due to receive radioactive material from these ageing legacy facilities and the discrepancy is exacerbated by conservative assumptions for waste swell due to insufficient understanding of gas retention. The physics of gas retention and release has also provoked interest and research outside of nuclear

decommissioning [8-10]; most notably the growth and release of methane bubbles formed by microbial decomposition in marine soft sediments contributes significantly to global greenhouse gas levels [9]. Nonetheless, there is currently limited understanding of the mechanics of bubble formation, growth and rise in soft sediments [11].

This research combines an investigation of the mechanical properties and three phase interfacial behaviour of these soft sediments with insights from x-ray tomography of gas containing beds. In-situ gas generation in nuclear waste environments is approximated using the decomposition of hydrogen peroxide in magnesium hydroxide soft sediments at laboratory scale. The size and shape distributions of retained bubbles are observed under different sediment shear yield stress conditions.

2 Theory

Bubbles quickly grow to the scale of pores or capillaries within soft sediments, at which point the bubble encounters the sediment matrix and the mechanics of bubble growth will depart from those in conventional fluids [8]. No model relating subsequent bubble growth to the mechanics or rheology of the soft sediment has received widespread acceptance [12], however a number of growth mechanisms have been proposed for different sediment conditions [8]:

- Capillary invasion – When the growing bubble encounters the sediment matrix either the bubble will deform the sediment structure or the sediment will deform the bubble. Capillary invasion occurs when the sediment structure remains rigid and the bubble intrudes into the dendritic pore network. Capillary invasion is governed by the Young-Laplace equation [7], which implies that soft sediments with small grain sizes and thus small pore throat radii, r_{th}, will experience high pore entry pressures. Likewise, if the sediment is well wetted by the continuous phase, with negligible adhesion between solid and gas, this growth mechanism will be energetically unfavourable [8]. The Young-Laplace equation may be stated as:

$$\Delta P_{ci} = \frac{2\gamma}{r_{th}} \cos(\theta) \tag{2}$$

  where ΔP_{ci} is the excess bubble pressure required for capillary invasion, γ is the interfacial surface tension and θ is the three phase contact angle.

- Cavity expansion – If the bubble cannot invade the pore space the bubble may create space within the capillary network by expanding its host cavity; this mechanism is characterised by a more spherical, regular shaped bubble [5]. Cavity expansion theory, Equation (3), states that the greater the mechanical strength of the soft sediment, characterised according to its shear yield stress, τ, and shear modulus, G, the greater the resistance to cavity expansion [10]:

$$\Delta P_{ce} = \frac{4}{3}\tau \left(1 + ln\left|\frac{G}{\tau}\right|\right) \tag{3}$$

  where ΔP_{ce} is the excess bubble pressure required for cavity expansion.

- Tensile fracture – Highly consolidated soft sediments with both small grain sizes and high shear yield stresses are frequently encountered in natural marine sediments [11, 12] and longstanding nuclear legacy facilities [1-3], and so both of the above mechanisms will experience substantial resistance. Under such conditions, the tensile stress exerted by the growing bubble may cause the soft sediment to fracture if the combined compressive and tensile strengths of the sediment are exceeded. Since the compressive strength is weakest in the horizontal direction, normal to the lithostatic load, these fractures tend to propagate laterally through the sediment [8]. Jain and Juanes [13] proposed that the excess bubble pressure for fracture scales with the inverse square of the grain size, implying that fracture will be energetically favourable to capillary invasion in very fine grained sediments.

The available mechanisms for bubble release are coupled to those that govern bubble growth. Under conditions that favour tensile fracture, volatile diffusion towards cracks promotes gas transport to the walls of the vessel where it can be released. The merging of these cracks with each other and with drainage channels at the bed surface can lead to the formation of stable channels [10]. High yield stress soft sediments can support stable open channels to a greater depth than weaker beds and so stable channel formation is a more significant mode of gas release in sediments with shear yield stresses greater than 1 kPa [10, 14].

In weaker sediments conducive to bubble growth by cavity expansion the excess bubble pressure is able to overcome the mechanical strength of the sediment matrix. By analogy, a bubble of sufficient buoyant force could also overcome the bed yield stress and fluidise the sediment [8, 10]. The buoyant

force of the bubble is proportional to the density driving force between the gas, ρ_b, and soft sediment, ρ_s, and increases in proportion with bubble volume. If the strength of the bed is characterised according to its yield stress, a pressure term, the restraining force will be proportional to the product of this stress and the bubble cross sectional area. Hence, the ratio of yield stress to sediment bulk density defines a critical bubble diameter, $d_{b,crit}$, to which a bubble must grow before it can fluidise the soft sediment and rise through the bed [10]:

$$d_{b,crit} = Y\frac{\tau}{\rho_s g} \tag{4}$$

where Y is a material dependent dimensionless yield parameter. According to this definition, bubble release by fluidisation will be more prominent in low strength soft sediments with yield stresses of less than around 100 Pa and correspondingly low critical bubble diameters. Rise of individual bubbles by fluidisation can facilitate further bubble release through a bubble cascade [14], where local bubbles either in the path or wake of the rising bubble are liberated as the initial bubble escapes.

The capacity of beds to retain large void fractions of flammable gas and pose the risk of episodic buoyant releases is strongly influenced by the available mechanisms for gas release. With fluidisation and stable channel formation promoting gas release in weak and strong sediments, respectively, it is thought that intermediate strength beds in the yield stress range of 100-1000 Pa are susceptible to the greatest bed swell and therefore pose the greatest risk of episodic buoyant releases [14].

3 Methods

3.1 Test materials

The brucite, $Mg(OH)_2$, test material used in this study is H3 Versamag (Martin Marietta Magnesia Specialties LLC, USA), a fine white precipitated powder with less than 1.2 % oxide impurities [15]. The advertised median particle size is 1.09 µm [15], however light scattering particle size distribution (Malvern Mastersizer) reveals a median diameter of 4.4 µm, reflecting the tendency of magnesium hydroxide to rapidly aggregate in aqueous environments. Soft sediments are prepared by the addition of water and agitation for 30 mins using an overhead stirrer and axial flow impeller. In-situ gas generation was achieved by addition of 35 % w/w hydrogen peroxide which decomposes within the bed to form oxygen bubbles according to Equation (5). It is understood that although the composition, and hence solubility, of the gas may impact the observed bubble growth rates, it plays a limited role in the physics governing gas retention and release [12]. Consequently, oxygen bubbles were considered an acceptable analogue for hydrogen, while also benefitting from relatively controllable reaction kinetics.

$$H_2O_2 \rightarrow H_2O + \frac{1}{2}O_2 \tag{5}$$

3.2 Characterising the mechanical properties of the bed

The mechanical strength of the soft sediments is characterised according to their shear yield stress, which was determined using the vane method [16]. A Brookfield viscometer was used to rotate four blade vanes of either 6.3 or 10.8 mm diameter in the sediment at 0.5 rpm to observe the evolution of torque, T, with time. Thirty seven such torque-time correlations were obtained in the concentration range of 30-52 % w/w. The shear yield stress was determined from the maximum torque and vane dimensions according to Equation (6) [16]:

$$T_{max} = \frac{\pi D^3}{2}\left(\frac{H}{D} + \frac{1}{6}\right)\tau \tag{6}$$

where H and D are the height and diameter of the vane. Alderman et al. [17] and Sherwood and Meeten [18] both discuss the use of the torque-time correlation to determine the shear modulus in addition to the yield stress, which is relevant to the cavity expansion mechanism for bubble growth in Equation (3). The maximum gradient in the torque-time profile, combined with the angular velocity, ω, and dimensions of the vane can be used to determine the shear modulus according to Equation (7) [17]:

$$G = \frac{1}{4\pi\omega H}\left(\frac{dT}{dt}\right)_{max}\left(\frac{1}{R^2} - \frac{1}{R_c^2}\right) \tag{7}$$

where R and R_c are the radii of the vane and sample container.

3.3 Characterising the three phase interface

The air-water-brucite interface was studied using an 80 cm^2 Langmuir-Blodgett trough [19, 20] after preparing a magnesium hydroxide monolayer at the trough surface. The trough was repeatedly cleaned with methanol and millipore water and then suction dried until the surface pressure of the water-filled trough measured less than 0.3 mN m^{-1} after the barriers were closed. A 3.9 % w/w solution of magnesium hydroxide in isopropanol was sonicated for 10 min before the monolayer was prepared by pipetting 1 mL of the sonicated suspension to the surface of the trough using 500 µL micro-syringes. After allowing a 10 min period for the isopropanol to evaporate from the monolayer, the barriers were closed from 80 to 20 cm^2 and surface pressure was determined from a force balance on a Wilhelmy plate attached to a microbalance [20].

The Langmuir-Blodgett trough tests were complemented with Bikerman tests [21, 22] to test the foamability of magnesium hydroxide-water suspensions. Air was bubbled through suspensions of 2, 4 and 8 % v/v using a 46-60 µm pore fritted glass disk at the base of a 34 mm glass column. The column was calibrated to millimetre precision using adhesive measuring tape to measure the height of foam across a range of air flow rates up to 60.6 ml min^{-1}.

3.4 X-ray computed tomography

X-ray computed tomography (CT) has proven an effective means of observing retained bubbles in optically opaque soft sediments [11-12]. A 6.5 L volume of soft sediment was prepared and pumped to a 300 mm diameter, 150 mm long side mounted acrylic cylinder as shown in Figure 1. A relatively homogeneous distribution of hydrogen peroxide was achieved by injection during the preparation stage, point (1). Alternatively, a less homogeneous distribution of hydrogen peroxide was achieved by steady injection at point (2) during transfer to the test cylinder.

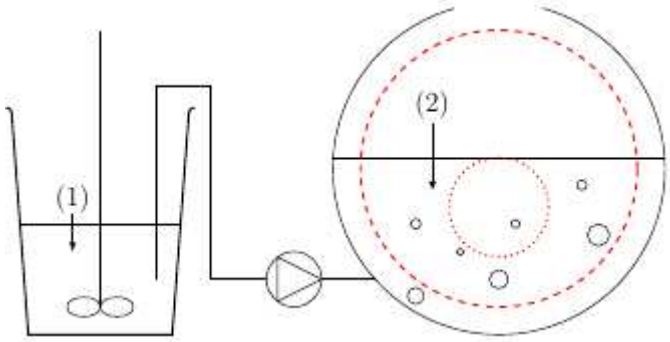

Figure 1: Schematic of x-ray tomography test apparatus demonstrating two alternative H_2O_2 injection points (1) and (2), and two imaging fields of view in red

Two fields of view (FOV) are highlighted in Figure 1. The smaller FOV was used to capture high resolution images over 8 hrs of gas generation. The lower resolution larger FOV was used to observe macro-features in the bed after 2 and 6 hrs of gas generation, thus providing a point of comparison between beds of different solids concentrations and hence different yield stress conditions. The key CT parameters are summarised in Table 1. CT tests were performed for beds of 30, 40, 45 and 54 % w/w $Mg(OH)_2$ concentration.

Table 1: X-ray CT parameters for two imaging fields of view

	Small FOV	Large FOV
X-ray voltage (kVp)	120	120
X-ray tube current (mA)	79	40
Field of view diameter (mm)	96	250
Field of view depth (mm)	20	140
Pixel dimensions (µm)	250	488
Slice separation (µm)	625	1250

Statistics of the retained bubble population were determined by three dimensional image analysis using FIJI-ImageJ software [23]. A stack of CT images was first thresholded to create binary images of black bubbles against white soft sediment using the Renyi entropy algorithm [24]. Discrete bubbles were then identified by inter-connecting the black voxels which were face, edge or corner adjacent using the algorithm in Bolte and Cordelières [25] and the volume, surface area and co-ordinates of each individual bubble were recorded.

4 Results and discussion

An example torque-time profile, acquired using the smaller Brookfield vane in a 45 % w/w magnesium hydroxide sample, is presented in Figure 2. The maximum torque and maximum first derivative of torque are shown using dashed lines to demonstrate the calculation of the shear yield stress and shear modulus. Power law fits with solids concentration, ω, generated the yield stress and shear modulus correlations in Equations (8) and (9), respectively:

$$\tau = 2.156 \times 10^5 \omega^{8.55} \quad (8)$$

and

$$G = 4.737 \times 10^4 \omega^{6.71} \quad (9)$$

This information enables full characterisation of the excess bubble pressure required for cavity expansion. However, in order to determine whether this represents the likely mechanism for bubble growth a better understanding of the air-water-brucite interface is required.

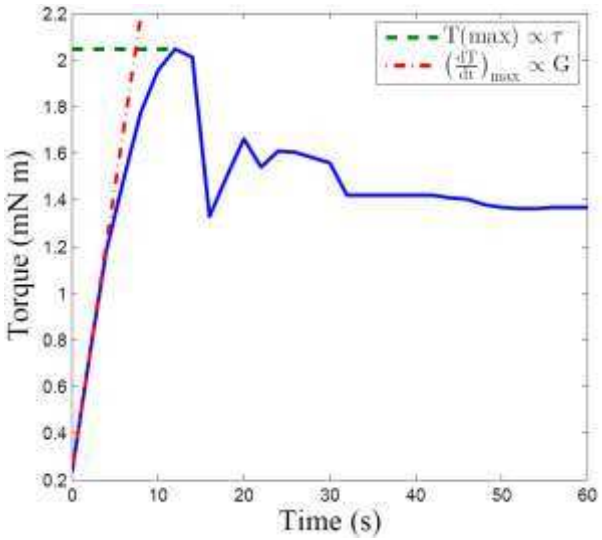

Figure 2: Torque-time profile for 45 % w/w magnesium hydroxide soft sediment

Figure 3 shows three Langmuir-Blodgett isotherms generated during compression-expansion cycles following identical monolayer preparation. Runs 2 and 3 are most comparable in shape, characterised by an increase in the surface pressure curve during the condensed phase until the monolayers collapse at pressures of 34.4 and 30.4 mN m^{-1} respectively and significant hysteresis between compression and expansion operation. Run 1 does not demonstrate such a clear yield point, however the increase in surface pressure and the hysteresis observed during expansion is similar to runs 2 and 3.

The maximum surface pressures following compression of 34-46 mN m^{-1} confirm the presence of a large number of surface active particles supported at the interface, while the hysteresis during the expansion cycle implies that the magnesium hydroxide monolayer is relatively inelastic. The dashed line at an area of 50.7 cm^2 represents the area that would be occupied at a perfect hexagonal packing arrangement of the added mass of 4.4 µm $Mg(OH)_2$ particles. The fact that the monolayers of runs 2 and 3 yield at 34-41 cm^2 surface coverage implies that around 20-33 % of the added solid is not supported at the interface and has fallen into the sub-phase, hence these particles have no finite contact angle. This hydrophilic particle behaviour is supported by Bikerman tests which demonstrated no foamability for suspensions of 2-8 % v/v. This does not preclude stable contact between solid and gas as Hunter, Wanless and Jameson [22] suggest that contact angles of at least 40°are required to form a stable foam. Furthermore the contact period between solid and gas during these dynamic tests may be insufficient for solids to stabilise at the interface and the timescales for bubble growth due to corrosion in nuclear silos will be much longer.

The test material has significant heterogeneity in its size distribution, it contains some oxide impurities and is likely to have a large standard deviation in surface roughness. This heterogeneity could account for the coexistence of hydrophilic behaviour and a significant number of surface active particles supported at the interface. Consequently, we cannot neglect the influence of stable contact between solid and gas on the physics of gas retention in magnesium hydroxide soft sediments.

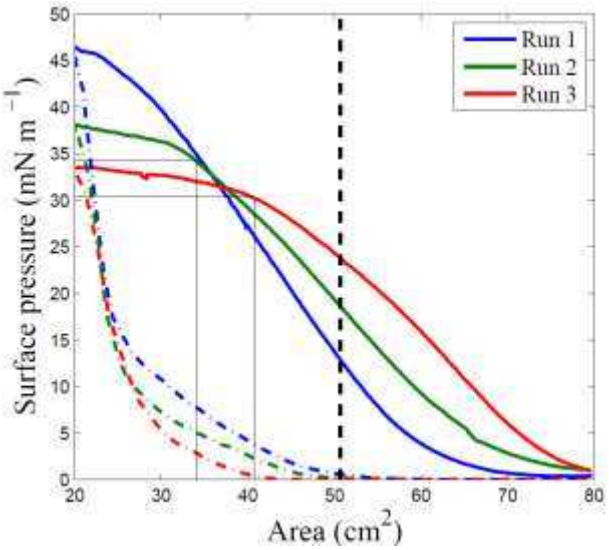

Figure 3: Langmuir-Blodgett isotherms for a magnesium hydroxide monolayer during compression (solid line) and expansion (dashed line)

The significance of the small 4.4 µm particle size and a broad range of three phase contact angles is that bubbles which are poorly contacted by solids within magnesium hydroxide soft sediments would experience very high capillary entry pressures. While cavity expansion becomes less energetically favourable with increased bed strength, even at a yield stress of 1 kPa a sediment with pore throats of 10 µm and a zero contact angle would require 178 times more energy to invade the capillary than to displace the local sediment matrix. Contact angles of at least 89.7° would be required b efore it would become energetically favourable to invade a pore of such small dimensions. Consequently, the dendritic bubbles associated with capillary invasion are unlikely to be prominent under realistic Sellafield waste conditions.

The absence of dendritic bubbles is confirmed in Figure 4, which presents an x-ray CT slice through a 54 % w/w sediment of 1112 Pa yield stress after 6 hrs of gas generation. The bubble geometries are either teardrop or ellipsoidal bubbles in the top region of the bed, consistent with bubble growth by visco-elastic cavity expansion, or lateral fractures in the deeper regions consistent with tensile fracture. The bulk sediment in the bottom third of the vessel appears brighter than the remainder of the bed, indicating a region of greater radiodensity and hence greater solids concentration. This, combined with the light swirls in the upper regions of the bed, reflects the difficulties in homogenising soft sediments with such a high solids content. It is interesting to note that cracks are especially prominent in the deeper and higher density regions where the sediment matrix will be more difficult to displace elastically, consistent with Boudreau et al. [12].

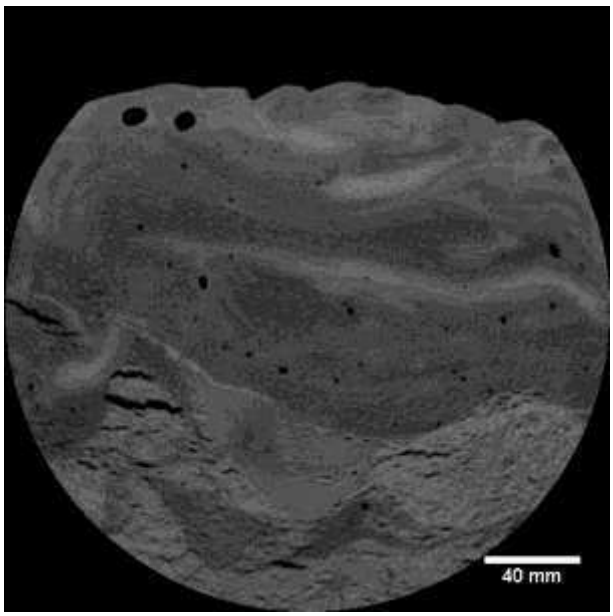

Figure 4: Example x-ray tomograph of 1112 Pa soft sediment after 6 hrs of gas generation

Figure 5 presents two CT slices through 7 Pa soft sediment after 6 hrs of gas generation. Figure 5a, like Figure 4, was obtained using mixing regime 1, where hydrogen peroxide was well distributed through the bed. The bubble geometries appear largely spherical, implying that cavity expansion is the dominant mode of bubble growth. The size distribution of bubbles is also significantly smaller than the population in Figure 4, owing to the smaller yield stress and hence the smaller critical bubble diameter required to fluidise the surrounding sediment according to Equation (3). Samples of 84 and 234 Pa yield stress demonstrated the same distribution of dispersed, regular shaped bubbles as Figure 5a.

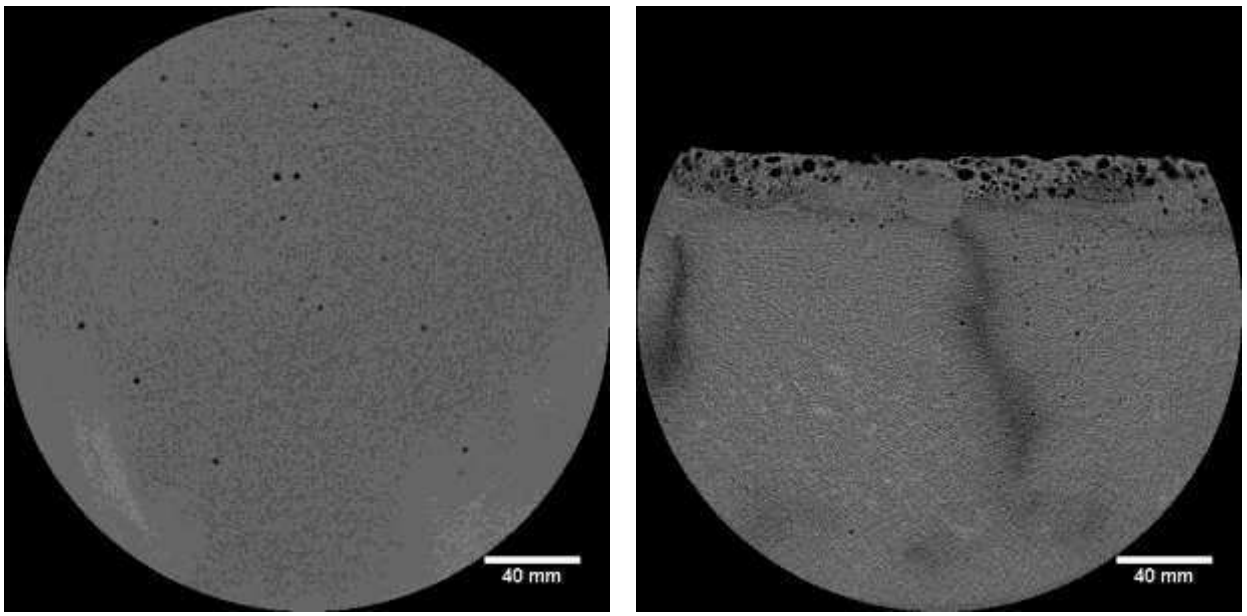

(a) Mixing regime 1 (b) Mixing regime 2

Figure 5: Example x-ray tomographs through 7 Pa soft sediment after 6 hrs of gas generation using alternative hydrogen peroxide mixing regimes.

Some more interesting macro-features become apparent in Figure 5b where the alternative injection route of hydrogen peroxide did not facilitate gas generation as homogeneously through the bed. The bed segregated into a bulk sediment and a foam layer with an especially high gas content in the top few centimetres of the bed. This foam layer is also able to support much larger bubbles than the bulk sediment. In the presence of a supernatant, as is the case in real waste environments, this foam layer

would certainly not be stable as its density is much less than that of water. This could result in a floating crust as observed in some underground waste tanks at Hanford [26]. Figure 5b suggests that a significant portion of magnesium hydroxide particles are able to stabilise a foam, however longer contact times are required than were achieved during the Bikerman tests. The presence of the foam layer supports the Langmuir-Blodgett trough tests which imply that interfacial science has a role to play in governing gas retention in these soft sediments.

Beneath the foam layer two distinct submerged dark regions rich in very small bubbles, close to voxel resolution, are visible. The further 111 slices taken through the bed reveal that these dark regions propagate throughout the bed and in all directions. These regions are considered to have originated from the large supersaturation of volatiles close to the point of hydrogen peroxide addition, thus leading to the nucleation of a large number of microbubbles. These low density regions are likely to provide preferential pathways for gas transport through the bed, to the walls of the vessel and to the foam layer. This could present a novel mechanism for gas release which would also explain why the void fraction of the bed in Figure 5b is much lower than that in Figure 5a after the same amount of gas has been generated within the bed. In real legacy wastes found in 50 year old silos, ponds and tanks, the beds will be highly chemically and physically heterogeneous and so non-uniform supersaturation of volatiles, as imaged in Figure 5b, could be more realistic to industrial process conditions than Figure 5a. Consequently, it would be reassuring if heterogeneous bubble nucleation and growth facilitated additional continuous gas release as this would limit undesirable waste swell during interim storage and make episodic buoyant release of flammable gas less likely.

Image analysis was conducted for beds of 7, 84, 234 and 1112 Pa yield stress, 6 hrs after hydrogen peroxide addition using mixing regime 1, long after the bubble size distribution had achieved steady state. Figure 6a shows bubble size distributions under each of the sediment conditions; bubbles comprised of fewer than 6 voxels were excluded from analysis as the number of very small bubbles was quite sensitive to thresholding and applying this lower limit ensured that only real features were analysed. The bubble size distributions of the three lowest strength beds are closely aligned, with no bubbles greater than 9 mm equivalent spherical diameter observed. Larger bubbles of up to 20 mm were stable in the 1112 Pa bed and the median bubble size of 5 mm was 70 % larger than observed in the lower yield stress beds.

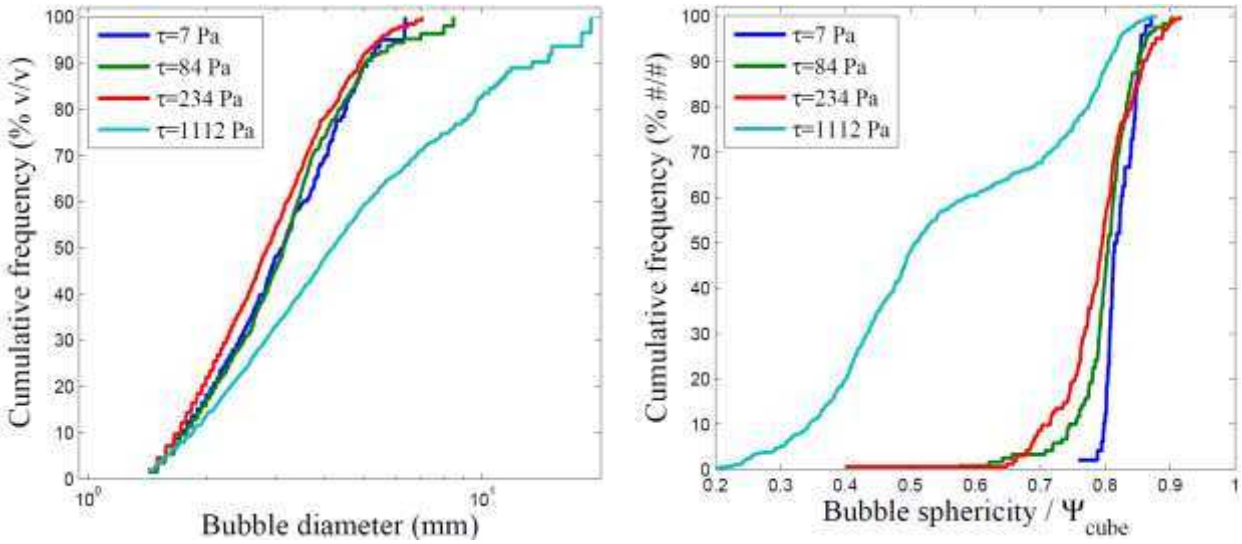

(a) Bubble size distribution for bubbles of at least 6 voxels

(b) Bubble shape distribution for bubbles of at least 80 voxels

Figure 6: Bubble statistics after 6 hrs bubble growth under different sediment yield stress conditions

Equation (3) implies that the ratio of yield stress to bulk bed density limits the maximum bubble size that can be retained by the bed as a result of fluidisation. This ratio increases by a factor of 28 in the yield stress range of 7 to 234 Pa, so it is surprising that no increase in retained bubble size is demonstrated in Figure 6a. However, analysing instantaneous bubble populations may bias the size distribution in favour of smaller bubbles which have longer residence times in the bed and are thus more likely to be captured. This will be addressed in future work with the use of dynamic scanning to track the motion of individual bubbles to better characterise bubble rise due to fluidisation.

Figure 6b provides shape analysis of retained bubble population. Theory suggests that it is easier for bubbles to displace low strength and shallow sediments isotropically, resulting in more regular shaped bubbles [12]. Very small bubbles have very high Laplace pressures which typically results in highly spherical bubbles and so shape analysis was limited to bubbles composed of at least 80 voxels. The shape is represented using a digital sphericity, Ψ_{dig}, calculated from the volume, V, and surface area, A, of the bubble and normalised against the sphericity of a cube, Ψ_{cube}, which cannot be exceeded by a digitised object comprised of voxels.

$$\Psi_{\mathrm{dig}} = \frac{\pi^{\frac{1}{3}}(6V)^{\frac{2}{3}}}{A}\left(\frac{6}{\pi}\right)^{\frac{1}{3}} = \frac{6}{A}V^{\frac{2}{3}} \tag{10}$$

The digital sphericity marginally decreases with increased yield stress in the 7-234 Pa yield stress range, supporting the theory of less isotropic bubble growth in higher strength sediments. There is a more significant decrease in bubble sphericity in the 1112 Pa bed, which exhibits a bimodal sphericity distribution. The two modes represent the distorted elliptical bubbles and the fractured cracks which are shown to co-exist at different locations in the bed in Figure 4. Further data in the 234-1112 Pa range would help to more precisely determine the conditions which mark the onset of bubble growth by tensile fracture, which appears to significantly limit the capacity for the bed to attain large voidages in excess of 25 %.

5 Conclusions and recommendations

Understanding the mechanisms which govern growth, retention and release of hydrogen bubbles in magnesium hydroxide soft sediments is crucial to safe decommissioning of legacy facilities at the Sellafield nuclear site. The fine grain size implies very high entry pressures for bubbles to invade the capillary network. The prevalence of more regular shaped bubbles, consistent with bubble growth by cavity expansion, is supported by x-ray tomographs of largely spherical bubbles of 1-9 mm diameter in 7-234 Pa yield stress beds. Further analysis of the retained bubble population demonstrated larger bubbles becoming progressively more distorted with increased bed strength due to increased anisotropy of stress in more consolidated beds. Increasing the bed yield stress to 1112 Pa facilitated the retention of much larger bubbles of up to 20 mm equivalent spherical diameter and a bi-modal sphericity distribution. This reflects the two modes of bubble growth apparent in the bed, with elliptical bubbles resulting from visco-elastic cavity expansion and elongated horizontal cracks resulting from tensile fracture.

CT experiments performed on beds with a less homogeneous supersaturation of volatiles identified various additional features, including a high voidage foam layer in the top few centimetres of the bed and dark regions, rich in microbubbles pervading throughout the sediment in all directions. These low density regions could provide preferential pathways for gas transport and release from sediments which are much too weak to support stable open channels and would explain the significantly reduced voidage as a result of this alternative methodology for gas generation. However, it should be recognised that dilution and homogenisation of nuclear legacy waste for transport during decommissioning is likely to enhance, rather than diminish the capacity of these soft sediments to retain large gas voidages in their new storage environment. Where it is not possible to dewater these wastes back to highly consolidated, high yield stress conditions that facilitate enhanced continuous gas release, ample ullage space should be provided in storage containers to prevent the accumulation of flammable concentrations of hydrogen.

Further work will focus on the transient behaviour of retained bubbles, with short interval, increased resolution tomography used to trace the growth, motion and distortion of the bubble population. Furthermore, the rheology and wetting behaviour of these soft sediments is better understood than their microstructure and so micro-CT analysis will be used to examine the dimensions and connectivity of the capillary structure.

Acknowledgements

The authors wish to thank the Engineering & Physical Sciences Research Council (EPSRC), the National Decommissioning Authority (NDA) and Sellafield Ltd. for sponsoring this research. Particular thanks to Geoff Randall and Martyn Barnes of Sellafield Ltd. for their support, to Samuel Allshorn and Carlos Grattoni for their x-ray tomography expertise and to Tony Windross for engineering the test rigs used in this study. We are grateful to the Armourers and Brasiers Gauntlet Trust for supporting our participation at Chemeca 2016 through a research travel grant.

References

1. McCracken, G. and Eilbeck, M. (2005) Clean up progress on high hazard facilities at Sellafield: Magnox swarf storage silos. In 2005 ANS Topical Meeting on Decommissioning, Decontamination, and Reutilization, vol. 2005, 161-167
2. Gregson, C. R., Goddard, D. T., Sarsfield, M. J., and Taylor, R. J. (2011) Combined electron microscopy and vibrational spectroscopy study of corroded Magnox sludge from a legacy spent nuclear fuel storage pond. Journal of Nuclear Materials, 412, 145-156
3. Burrows, R., Harris, S. and Stevens, N. (2005) Corrosion electrochemistry of fuel element materials in pond storage conditions. Chemical Engineering Research and Design, 83, 887-892
4. Kam, S., Gauglitz, P. and Rossen, W. (2001) Effective compressibility of a bubbly slurry. I. theory of the behaviour of bubbles trapped in porous media. Journal of Colloid and Interface Science, 241, 248-259
5. Kam, S., Gauglitz, P. and Rossen, W. (2001) Effective compressibility of a bubbly slurry. II. fitting numerical results to field data and implications. Journal of Colloid and Interface Science, 241, 260-268
6. Allemann, R. (1992) Physical mechanisms contributing to the episodic gas release from Hanford tank 241-SY-101. In High Level Radioactive Waste Management 92, Las Vegas
7. Kam, S. I., and Rossen, W. R. (1999) Anomalous capillary pressure, stress, and stability of solids-coated bubbles. Journal of Colloid and Interface Science, 213, 329-339
8. Boudreau, B. (2012) The physics of bubbles in surficial, soft, cohesive sediments. Marine and Petroleum Geology, 38, 1-18
9. Katsman, R., Ostrovsky, I. and Makovsky, Y. (2013) Methane bubble growth in fine-grained muddy aquatic sediment: Insight from modeling. Earth and Planetary Science Letters, 377-378, 336-346
10. Van Kessel, T. and Van Kesteren, W.G.M. (2002) Gas production and transport in artificial sludge depots. Waste Management, 22, 19-28
11. Algar, C. K., Boudreau, B. P. and Barry, M. A. (2011) Initial rise of bubbles in cohesive sediments by a process of viscoelastic fracture. Journal of Geophysical Research: Solid Earth, 116(B4)
12. Boudreau, B.P., Algar, C., Johnson, B.D., Croudace, I., Reed, A., Furukawa, Y., Dorgan, K.M., Jumars, P.A., Grader, A.S. and Gardiner, B.S. (2005) Bubble growth and rise in soft sediments. Geology, 33, 517-520
13. Jain, A.K. and Juanes, R. (2009) Preferential mode of gas invasion in sediments: Grain-scale mechanistic model of coupled multiphase fluid flow and sediment mechanics. Journal of Geophysical Research: Solid Earth, 114(B8)
14. Gauglitz, P. A., Bontha, J.R., Daniel, R.C., Mahoney, L.A., Rassat, S.D., Wells, B.E., Bao, J., Boeringa, G.K., Buchmiller, W.C., Burns, C.A. and Chun, J. (2015) Hydrogen Gas Retention and Release from WTP Vessels: Summary of Preliminary Studies (No. PNNL-24255). Pacific Northwest National Laboratory (PNNL), Richland, WA (US)
15. Magnesium hydroxide MSDS (2014) CAS # 1309-42-8. Martin Marietta Magnesia Specialties
16. Dzuy, N.Q. and Boger, D. (1985) Direct yield stress measurement with the vane method. Journal of Rheology 29, 335-347
17. Alderman, N., Meeten, G. and Sherwood, J. (1991) Vane rheometry of bentonite gels. Journal of Non-Newtonian Fluid Mechanics, 39, 291-310
18. Sherwood, J. and Meeten, G. (1991) The use of the vane to measure the shear modulus of linear elastic solids. Journal of Non-Newtonian Fluid Mechanics, 41, 101-118
19. Ybert, C., Lu, W., Möller, G. and Knobler, C.M. (2002) Collapse of a monolayer by three mechanisms. Journal of Physical Chemistry B, 106, 2004-2008
20. Derkach, S.R., Krägel, J. and Miller, R. (2009) Methods of measuring rheological properties of interfacial layers (experimental methods of 2D rheology). Colloid Journal, 71, 1-17
21. Tan, S.N., Pugh, R.J., Fornasiero, D., Sedev, R. and Ralston, J. (2005) Foaming of polypropylene glycols and glycol/MIBC mixtures. Minerals Engineering, 18,179-188
22. Hunter, T.N., Wanless, E.J. and Jameson, G.J. (2009) Effect of esterically bonded agents on the monolayer structure and foamability of nano-silica. Colloids and Surfaces A: Physicochemical and Engineering Aspects, 334, 181-190.
23. Schindelin, J., Arganda-Carreras, I., Frise, E., Kaynig, V., Longair, M., Pietzsch, T., Preibisch, S., Rueden, C., Saalfeld, S., Schmid, B. and Tinevez, J.Y. (2012) Fiji: an open-source platform for biological-image analysis. Nature methods, 9, 676-682.
24. J.N. Kapur, P.K. Sahoo and A.K. Wong (1985) A new method for gray-level picture thresholding using the entropy of the histogram. Computer Vision, Graphics, and Image Processing, 29, 273-285
25. S. Bolte and F.P. Cordelières (2006) A guided tour into subcellular colocalization analysis in light microscopy. Journal of Microscopy, 224, 213-232
26. Bryan, S., Pederson, L. and Scheele, R. (1992) Crust growth and gas retention in synthetic Hanford waste. In Waste Management 92, Tuscon

Presenting author biography

Michael Johnson is a Chemical Engineer from Cornwall, England undertaking PhD research at the University of Leeds on flammable gas retention within historic nuclear waste. His focus lies in rheological characterisation and x-ray computed tomography analysis. After studying for a Bachelor's degree in Chemical Engineering at the University of Manchester, Michael completed a Master's with Distinction at the University of Leeds, specialising in heat transfer in batch reactors.